2022

Thermodynamic Evaluation of a Magnetic Air Conditioner

Guilherme Peixer

Maria Cláudia Silva

Anderson Lorenzoni

Gislaine Hoffmann

Diego dos Santos

See next page for additional authors

Evaluating the Performance of a TRL-6 Magnetic Air Conditioner Prototype

Guilherme F. PEIXER*, Maria C. R. SILVA, Anderson LORENZONI, Gislaine HOFFMANN, Diego dos SANTOS, Sergio L. DUTRA, Hígor TEZA, Elias PAGNAN, Bernardo P. VIEIRA, Alan T. D. NAKASHIMA, Jaime A. LOZANO, Jader R. BARBOSA Jr.

POLO - Research Laboratories for Emerging Technologies in Cooling and Thermophysics
Department of Mechanical Engineering, Federal University of Santa Catarina
Florianópolis, SC, Brazil
Phone: + 55 48 3721 7886

* Corresponding Author: guilherme.peixer@polo.ufsc.br

ABSTRACT

This paper presents preliminary results of a magnetic air conditioner prototype tested in a relevant environment compatible with the Technology Readiness Level (TRL) 6. The prototype, which contains all components of a functional cooling system, was experimentally evaluated in an especially developed calibrated calorimeter designed according to international technical standards for testing split-type air-conditioning units. Although the preliminary performance parameters are below values currently exhibited by commercially available air conditioners, the prototype has achieved one of the largest temperature spans and cooling capacities among the magnetic refrigerators presented in the literature. In addition, the study sheds some light on the external irreversibilities associated with the heat exchangers, which can be highly detrimental to the system's performance and must be taken into account in the design and analysis stages.

1. INTRODUCTION

The most widely applied technology employed in refrigeration systems relies on a combination of mechanical compression and expansion of a vapor and phase change heat transfer. After more than a century of development, vapor compression is a mature technology with efficient and compact systems and a solid supply chain. However, the phase-out and phase-down of the volatile refrigerants employed in those systems, coupled with the demands from regulators and society for more efficient operation, stimulates the refrigeration community to explore alternatives to overcome such issues (Gauß et al., 2017). Among several options, Magnetocaloric Refrigeration (MR) stands out as one of the most promising not-in-kind cooling techniques (Qian et al., 2016). The main factors that attract interest from industry and academia towards MR are: (i) the use of a solid refrigerant and absence of harmful gases; (ii) the potential to achieve high thermodynamic efficiencies by combining factors such as the reversibility of the magnetocaloric effect (MCE) and recovery of magnetization work; and (iii) the possibility of recycling both the permanent magnets and the magnetocaloric materials (MCM).

Many lab-scale prototypes have been designed and commissioned around the world over the last decades (Greco et al., 2019). Recently, Nakashima et al. (2021) developed a magnetic wine cooler prototype with all the fundamental components required to operate the refrigeration system. The system achieved an operating point compatible with the system specifications, even though the power consumption was severely affected by viscous losses in an oversized pump, resulting in a maximum coefficient of performance, *COP*, of 0.38. Dall'Olio et al. (2021) developed a large-scale MR system, achieving a maximum *COP* of 6.7. However, the power consumption was estimated considering only the regenerator pumping power (given by the product of the pressure drop and volume flow rate through the porous media) and magnetic power (calculated as the product of the angular velocity of the magnetic rotor and the difference between the torques measured with and without a temperature span along the regenerator beds). Discrepancies between performance figures are common among reported MR prototypes (Greco et al., 2019) and cannot be attributed only to different operating conditions and design characteristics. More often than not, pump, motor, valve and heat exchanger losses are overlooked in the evaluation procedures set forth by various authors, giving rise to misleading expectations about the technology.

Even after decades of research and development, MR is not yet commercially available, and the prototypes developed so far did not achieve the expected performance targets (Kamran et al., 2020). Moreover, MR prototypes usually employ

electric heaters or thermal baths to emulate the thermal reservoirs, disregarding the influence of heat exchanger (HEx) losses, and do not consider other losses such as hydraulic valves, mechanical transmission and pumping efficiencies. In this context, this paper aims to perform an experimental thermodynamic evaluation of an MR prototype designed to operate as an air conditioner (AC). The Magnetic Refrigeration Unit (MRU) was developed using a system-level multi-objective optimization of the four main subsystems (Peixer, 2020): Active Magnetic Regenerator (AMR), Magnetic Circuit (MC), HEx and Hydraulic System (HS). In addition, an in-house calorimeter was designed, commissioned and calibrated to carry out the experimental tests (Silva et al., 2021). The system performance was evaluated in terms of the cooling capacity, coefficient of performance and second-law efficiency.

2. EXPERIMENTAL WORK

The experimental evaluation of the magnetic refrigeration system was carried out according to International (ISO-5151, 2017) and Brazilian (Inmetro, 2011, 2012, 2013) standards used to test vapor-compression air conditioners. After a detailed description of the calibrated calorimeter, this section presents the MRU and its components.

2.1 Calibrated Calorimeter

The development of a calibrated calorimeter was necessary to demonstrate the potential of magnetocaloric cooling technology in a relevant environment. Unfortunately, not all specifications could be met due to space and budget restrictions. However, that was not considered an impediment to the analysis as most parameters, particularly the tolerances of the measuring instruments, were within a margin deemed adequate to the project's objective, which is to characterize the system experimentally and not certify it according to technical standards. This paper briefly describes the calorimeter and its calibration process. Further details regarding the thermal design of the calorimeter can be found in Silva et al. (2021).

The calorimeter consists of two chambers separated by an insulated wall to emulate the outdoor (warm) and indoor (cold) conditions. The external dimensions of the calorimeter, along with the internal dimensions of the indoor and outdoor chambers, are presented in Table 1. All insulated walls are made of Polyisocyanurate, which has a thermal conductivity between 0.02 and 0.03 W/(m K); the wall that separates the indoor and outdoor chambers has a thickness of 150 mm, whereas the remaining walls are 70-mm thick. Pictures of the indoor and outdoor chambers are presented in Figure 1.

Table 1: Dimensions of the calorimeter.

Dimensions	Width [mm]	Length [mm]	Height [mm]
External - calorimeter	2200	4860	2640
Internal - indoor chamber	2060	2380	2490
Internal - outdoor chamber	2060	2190	2500

The indoor chamber is equipped with temperature and humidity reconditioning systems, whereas only the temperature is reconditioned in the outdoor chamber. The indoor chamber reconditioning system consists of electric heaters for temperature control, heaters immersed in water reservoirs for humidity control, and fans to homogenize the temperature and humidity. The outdoor chamber reconditioning system consists of a fan coil unit connected to a chiller. No pressure equalization device is employed. The reconditioning equipment of both chambers is summarized in Table 2.

Table 2: Reconditioning equipment employed in the calorimeter.

Equipment	Quantity	Specifications
Electric Heaters	8	Capacity of 1750 W each
Immersion heaters	4	Capacity of 1000 W each
Water reservoir	2	Stainless steel tanks, housing 30 liters of water each
Fans	5	Axial fans, with a nominal power of 200 W
Fan Coil unit	1	Cooling capacity of 30000 Btu/h
Chiller	1	Connected to the fan coil unit

The indoor and outdoor chambers are equipped with nine thermocouples, eight humidity transducers, and one pressure transducer. The wet-bulb temperatures are calculated based on the chambers' temperature, humidity, and pressure

(a) (b)

Figure 1: Calibrated calorimeter developed to evaluate the performance of the magnetocaloric air conditioner. (a) Indoor chamber, (b) outdoor chamber. The vapor compression evaporator and condensing unit shown in (a) and (b) were evaluated during the validation of the calorimeter.

measurements. The external ambient temperature is measured by seven thermocouples, and a thermo-hygrometer measures the ambient humidity. Two power transducers with full scales of 1000 and 2000 W measure the electric power of the heaters and fans. A calibrated scale measures the condensate mass, and temperature measurements are done in the immersion heater and condensate reservoirs. The uncertainties associated with each measurement carried out in the calorimeter are depicted in Table 3.

Table 3: Experimental uncertainties of the measuring instruments installed in the calorimeter.

Measurement	**Equipment**	**Uncertainty**
Water temperature	Thermocouple	± 0.25°C
Air dry bulb temperature	Thermocouple	± 0.25°C
Air dry bulb temperature	Thermo-hygrometer	± 0.12°C
Air relative humidity	Humidity transducers	± 2.8 %
Air relative humidity	Thermo-hygrometer	± 2 %
Electric Power	Power transducers (1000 W)	± 3.6 W
Electric Power	Power transducers (2000 W)	± 3.6 W
Pressure	Pressure Transducers	± 2 kPa
Mass	Scale	± 0.1 g

Heat leaks through the insulated walls must be accounted for in the characterization of AC systems in a calibrated calorimeter (ISO-5151, 2017). Therefore, a calibration was performed, which consisted of applying a thermal load using electric heaters in the chambers at steady-state, with a temperature difference between the chambers and the outside of at least 11 K. With the known values of the wall heat transfer rate and temperature difference, the overall calorimeter thermal conductance, *UA*, can be calculated. Moreover, the overall heat transfer coefficient, *U*, can also be calculated since the heat transfer area is known. This procedure is repeated three times: first, heating the indoor chamber only, then heating the outdoor chamber only, and, finally, both chambers simultaneously to determine the *UA*

values of each chamber and dividing wall, as shown in Table 4.

Table 4: Results of the calibration procedure.

Wall	UA [W/(K)]	U [W/(m^2 K)]
Dividing wall	1.7 ± 0.1	0.313 ± 0.016
Indoor chamber walls	13.9 ± 0.1	0.482 ± 0.005
Outdoor chamber walls	17.7 ± 0.1	0.779 ± 0.005

2.2 Magnetic Refrigeration Unit

MR systems are composed of four main subsystems: AMRs, MC, HEx and HS. There are several possible configurations for each of them, each with its advantages and disadvantages. A multidisciplinary team designed the prototype, and a patent has been filed (Lozano et al., 2021). MC consists of a rotor-stator configuration, known to achieve some of the highest cooling capacities in the literature (Trevizoli et al., 2016). This arrangement consists of two concentric cylinders separated by an air gap. The inner cylinder, or stator, is made from laminated sheets of soft ferromagnetic (electrical steel). The outer cylinder, or rotor, is made from blocks of soft ferromagnetic material and permanent magnets and rotates at a specified frequency. The maximum magnetic flux density achieved by the MC at the center of the radial magnetic gap is approximately 1.2 T.

In the AMRs positioned in the air gap between the rotor and the stator, the MCM functions as the refrigerant and regenerative matrix in a porous bed crossed by alternating fluid flows. In this way, a temperature difference is built up along the AMR beds, several times greater than the adiabatic temperature change of the material. The MCM consists of particles of Gd and $La(FeMnSi)_{13}H_z$ materials (commercialized as *Calorivac-HS2*) arranged in layers, forming a packed porous medium. Each AMR bed contains approximately 320 g of Gd and 950 g of *Calorivac-HS2*, housed by a stainless steel casing shaped as a sector of a hollow cylinder. The MC-AMR configuration is presented in Figure 2. Although the prototype has been designed and built to operate with sixteen regenerators, only eight AMR beds were employed in this preliminary study.

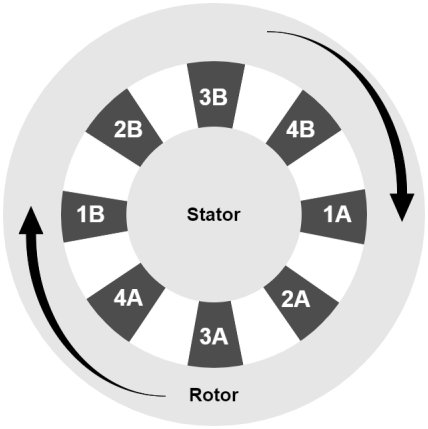

Figure 2: Schematic representation of the eight AMRs positioned in the air gap. AMRs with the same number are magnetized (and demagnetized) at the same time as the MC rotates clockwise.

The HS is driven by a gear pump assisted by solenoid valves, check valves and manifolds (Santos et al., 2021) according to the diagram presented in Figure 3. Each pair of solenoid valves controls a couple of AMRs with the same number in Figures 2 and 3.

Temperature and pressure are measured at several points along the hydraulic circuit, as indicated in Figure 3. The mass flow rate is measured at the inlets of the cold and hot HEx. The rotor is equipped with torque and power meters, which are also used to measure the fan power at the cold and hot HEx. An encoder and a Hall-effect sensor measure the rotor's magnetic flux density and angular position. The uncertainties associated with the measuring instruments installed in the MRU are presented in Table 5.

Due to their favorable thermal-hydraulic characteristics, fan-supplied multi-circuited herringbone-wave tube-fin HExs

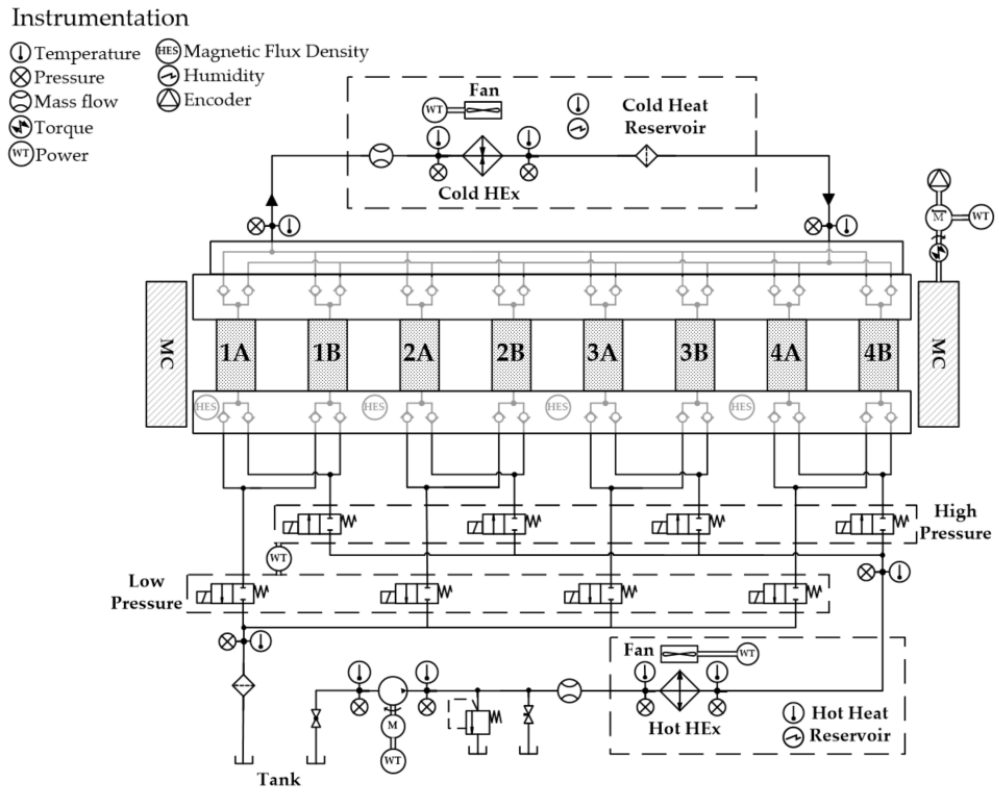

Figure 3: Hydraulic diagram of the magnetocaloric refrigeration unit (MRU).

Table 5: Experimental uncertainties of the measuring instruments installed in the MRU.

Measurement	Transducer	Uncertainty
Fluid temperature	Thermocouple	± 0.11°C
Air temperature	Thermocouple	± 0.11°C
Fluid pressure	Pressure transducer	± 0.01 bar
Torque	Torquemeter	≤ ± 0,25 Nm
Power consumption	Power transducer	± 3,5 W
Liquid mass flow rate (cold HEx)	Coriolis flow meter	± 6,8 kg/h
Liquid mass flow rate (hot HEx)	Turbine flow meter	± 1 %

were used to transfer heat between the fluid and the indoor and outdoor chambers (Peixer et al., 2022). The coupling between the AMR, cold and hot HEx and thermal reservoirs is illustrated in Figure 4. In addition, two temperature spans are in the figure, namely the regenerator temperature span, ΔT_{reg}, and the system temperature span, ΔT_{sys}. Note that the former is always larger than the latter due to the temperature differences in the heat exchangers. Note also that most MR prototypes do not employ actual heat exchangers; instead, thermal loads are produced by Joule-effect heaters (Kitanovski et al., 2015). Hence, a considerable thermal loss in current refrigeration systems is not considered in most MR prototypes developed so far.

The MRU and its components, except the cold HEx, are placed in the outdoor calorimeter chamber. A rendering of the whole unit is depicted in Figure 5; an explanatory video presenting the MRU operation in detail, including the calorimeter, can be found in the following link: https://bit.ly/2ZmbKFI.

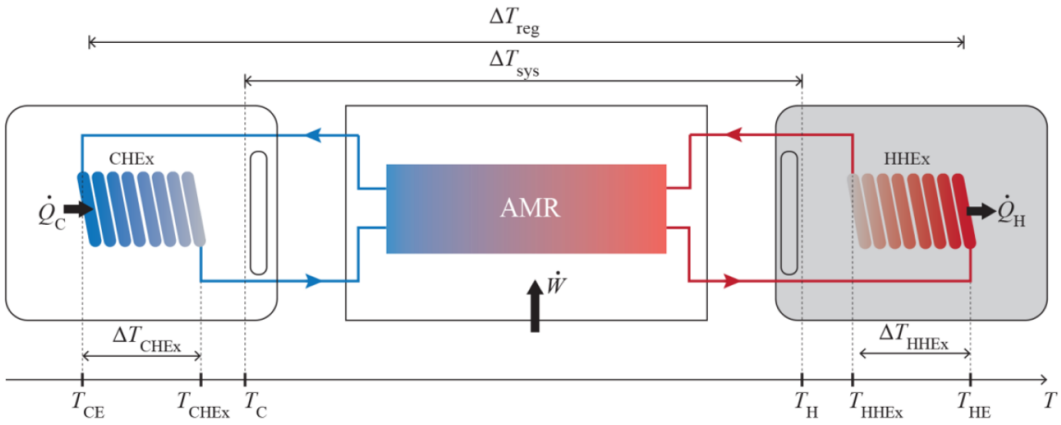

Figure 4: Schematic coupling between the AMR, cold and hot HEx and thermal reservoirs (indoor and outdoor chambers).

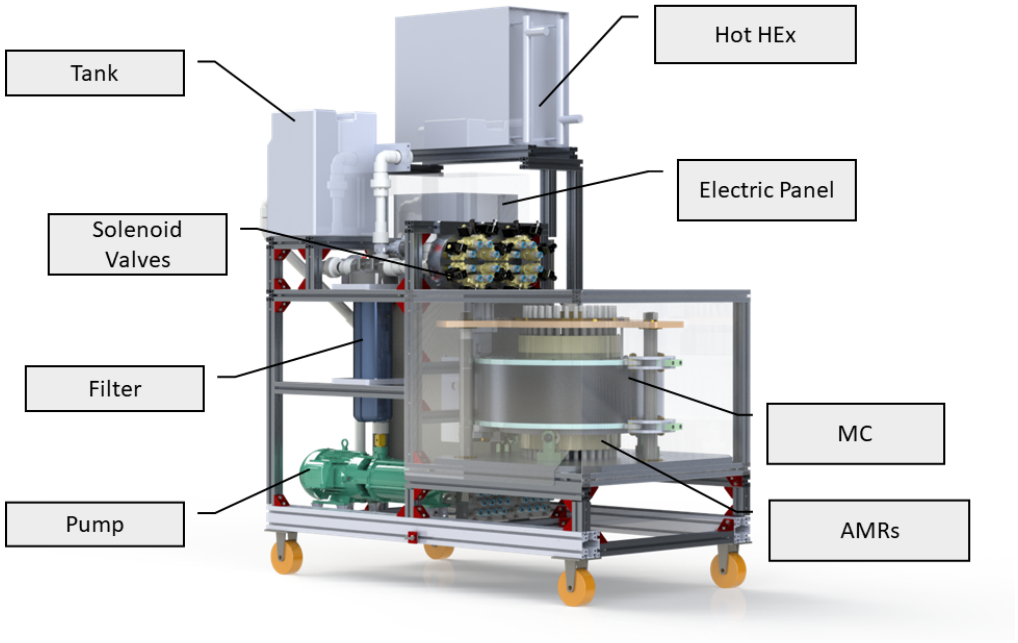

Figure 5: Schematic representation of the MRU and its main components.

2.3 Thermodynamic Performance Metrics

The performance of the system is evaluated in terms of the temperature spans (AMR and system), cooling capacity, $\dot{Q}_C$, *COP* and second law efficiency, η. The parameters associated with the AMR are better suited for comparison with other MR systems, while those associated with the system are better suited for comparison with other vapor compression systems. According to Fig. 4, the temperature span of the regenerators, ΔT_{reg}, and of the system ,ΔT_{sys}, can be calculated by:

$$\Delta T_{reg} = T_{HE} - T_{CE} \tag{1}$$

$$\Delta T_{sys} = T_H - T_C \tag{2}$$

where ΔT_{reg} is the difference between the temperature at the hot end of the AMRs, T_{HE}, taken as the temperature of the fluid in the outlet manifold of the hot side, and at the cold end, T_{CE}, measured at the same spot on the cold side. Conversely, ΔT_{sys} is defined as the difference between the outdoor temperature, T_H, determined from an average of the temperature measurements in the outdoor chamber, and the indoor temperature, T_C, also given by an average of the indoor chamber temperature measurements.

The cooling capacity of the AMR, $\dot{Q}_{C,reg}$, and of the system, $\dot{Q}_{C,sys}$, can be calculated, respectively, by:

$$\dot{Q}_{C,reg} = \dot{m}_f c_p \Delta T_{C,reg} \tag{3}$$

$$\dot{Q}_{C,Sys} = \dot{W}_{fn} + \dot{W}_{ht} + \dot{Q}_{wl} \tag{4}$$

where in Eq. (3) $\dot{m}_f$ is the fluid mass flow rate, c_p is the specific heat of water and $\Delta T_{C,reg}$ is the temperature difference between the fluid entering and exiting the cold end of the AMR, measured in the manifolds on the cold side. In Eq. (4), $\dot{W}_{fn}$ represents the power supplied to the fans, $\dot{W}_{ht}$ is the power to the heaters and $\dot{Q}_{wl}$ is the heat gain through the walls of the inner chamber. Since the liquid did not reach the air's dew point, no condensation and latent heat contribution was involved.

The *COP* of the AMR, COP_{reg}, and the *COP* of the system, COP_{Sys}, can be calculated by:

$$COP_{reg} = \frac{\dot{Q}_{C,reg}}{\Delta P_{reg}\dot{V}_l + \tau\omega} \tag{5}$$

$$COP_{Sys} = \frac{\dot{Q}_{C,Sys}}{\dot{W}_{pp} + \dot{W}_{rt} + \dot{W}_{CHEx} + \dot{W}_{HHEx} + \dot{W}_{SV}} \tag{6}$$

where, in Eq. (5), ΔP_{reg} is the AMR pressure drop (calculated at the manifolds), $\dot{V}_l$ is the liquid volume flow rate, τ is the torque and ω is the angular speed. In Eq. (6), $\dot{W}_{rt}$ is the power consumption to drive the rotor, $\dot{W}_{pp}$ represents the power consumption of the hydraulic pump, $\dot{W}_{CHEx}$ and $\dot{W}_{HHEx}$ are the power consumption contributions of the fans in each heat exchanger. Finally, $\dot{W}_{SV}$ is the power required to operate the solenoid valves.

Lastly, the second-law efficiency of the AMR, η_{reg} (internal), and the second-law efficiency of the system, η_{Sys} (external), are calculated by:

$$\eta_{reg} = COP_{reg}\frac{T_{HE} - T_{CE}}{T_{CE}} \tag{7}$$

$$\eta_{Sys} = COP_{Sys}\frac{T_H - T_C}{T_C} \tag{8}$$

3. THERMODYNAMIC PERFORMANCE ASSESSMENT

The performance of the MRU was evaluated at five different mass flow rates, ranging from 600 to 1400 kg/h. For each mass flow rate, the system was tested at two operating points defined by a thermal load (set by electric heaters in the indoor chamber) and a temperature span, where the outdoor temperature T_H was fixed at 35°C. Note that, at a given time, the mass flow rate is split between the regenerator pair (A and B) with the same number in Fig. 2. The blow fraction was set at 25%, and the operating frequency was kept fixed at 0.6 Hz, less than the design value of 1.6 Hz. It is expected that the system will be able to perform at the design frequency when the sixteen AMRs (full load) are installed; at the half-load condition of eight AMRs, magnetic cogging effects are still significant, which increases both the torque and power consumption.

The cooling capacity and temperature span as a function of the mass flow rate for the system and the AMR are presented in Figure 6. It is clear from Figure 6(a) that the system's response is best at 1200 kg/h, but the system, at this preliminary stage, is still incapable of delivering a suitable operating point for air-conditioning applications. However, looking at the AMR performance only (i.e., excluding the external losses) shown in Figure 6(b), from a perspective of comparing the present results with other MR prototypes presented in the literature, the performance is similar to the system recently developed by Masche et al. (2022).

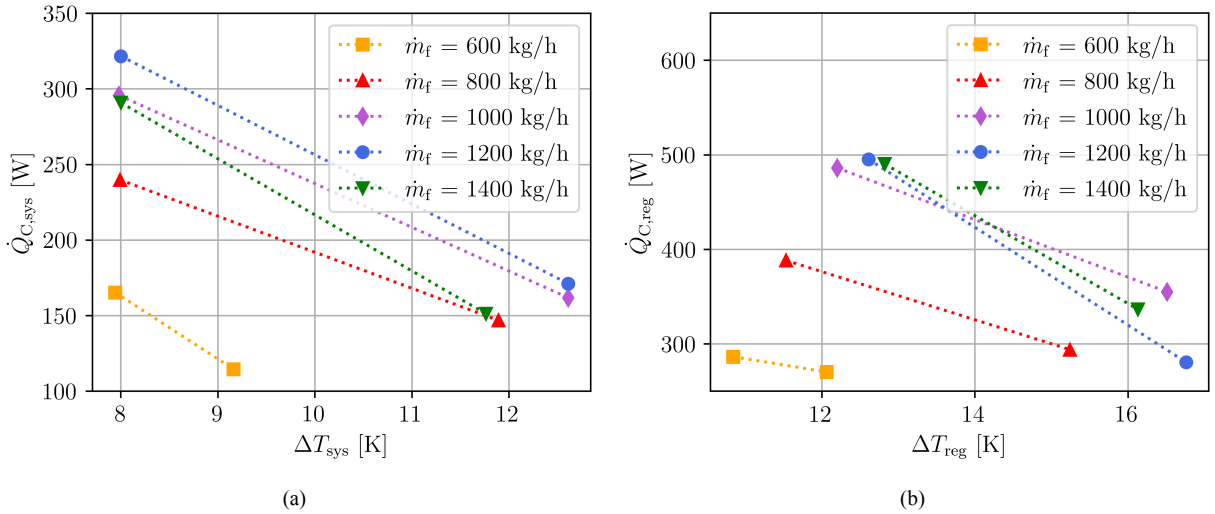

Figure 6: Cooling capacity and temperature span as a function of the mass flow rate for (a) the system and (b) the AMR.

When comparing both figures, the considerable influence of the heat exchangers on the system's performance becomes apparent. First, the temperature span is reduced by approximately 3 or 4 K due to the finite thermal conductances of heat exchangers. Other sources of irreversibility are dead volume and fluid mixing effects that decrease the cooling capacity at the cold end of the AMR. The cooling capacity is also reduced by thermal leaks in the tubing between the manifolds and the indoor chamber of the calorimeter. Hence, it becomes clear that, to evaluate MR prototypes properly, one must consider the influence of the heat exchangers on the cooling capacity and temperature span.

Figure 7 evaluates the behavior of the system and AMR thermodynamic efficiency in terms of the *COP* and η. Firstly, in absolute terms, it is evident that, in addition to the cooling capacity and temperature span, the power consumption and efficiency obtained in the preliminary tests are still below the requirements for practical applications of such systems. However, when the influence of the heat exchangers and other non-AMR power consumption factors are excluded from the analysis, Fig. 7(b), a threefold increase of the *COP* and η is observed, demonstrating a potential for improving the performance of the prototype.

4. CONCLUSIONS

Preliminary results of a magnetic air conditioner prototype were presented and discussed in this paper. In addition to the MRU, the calibrated calorimeter's main components, design, and operation were described in detail. The main performance results encountered so far demonstrated that the MR prototype should be improved in terms of cooling capacity, power consumption, and efficiency to be used commercially as an AC system. However, compared to other MR systems presented in the literature, the present prototype, to our knowledge, has reached one of the highest cooling capacities and temperature spans published in the literature. Further improvements in the prototype are expected to enhance the cooling capacity, temperature span, power consumption, and efficiency. The effect of external irreversibilities in MR systems has also been evaluated; their impact is highly detrimental to these systems, and they must be considered when designing or assessing the performance of not-in-kind technologies.

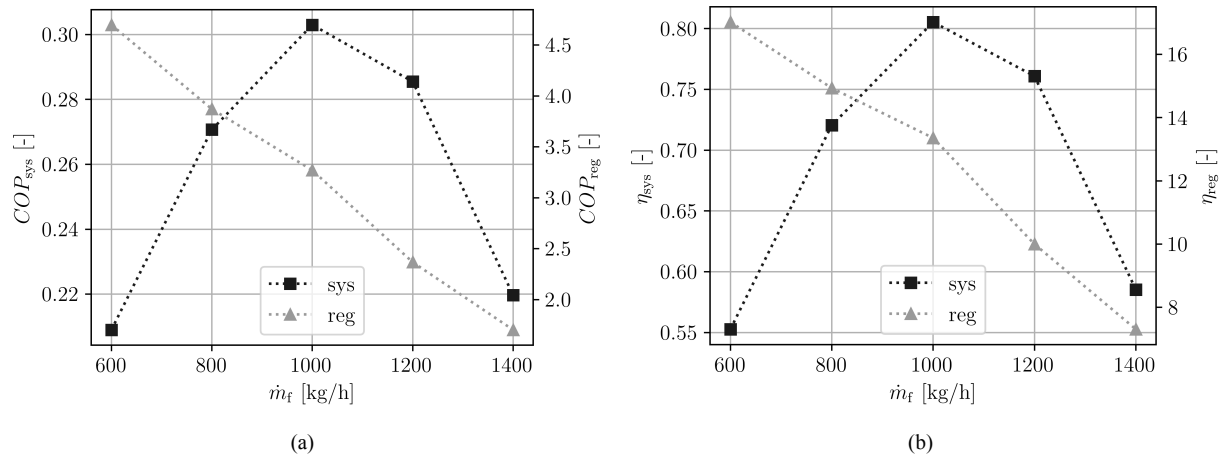

Figure 7: Results for (a) *COP* and (b) η for the AMR and system as a function of the mass flow rate.

NOMENCLATURE

A	area	(m^2)
c	specific heat	(J/(kg K))
$\dot{m}$	mass flow rate	(kg/h)
P	pressure	(Pa)
$\dot{Q}$	heat transfer rate	(W)
T	temperature	(K)
U	overall heat transfer coefficient	(W/(m^2 K))
UA	overall thermal conductance	(W/K)
$\dot{V}$	volumetric flow rate	(kg/h)
Δ	difference	(-)
τ	torque	(N.m)
ω	angular speed	(rad/s)

Subscript

C	cold
CE	cold end
CHEx	cold heat exchanger
fn	fan
H	hot
HE	hot end
HHEx	hot heat exchaner
ht	heaters
l	liquid
p	constant pressure
pp	pumping
reg	regenerator
rt	rotor
sv	solenoid valve
sys	system
wl	wall

REFERENCES

Dall'Olio, S., Masche, M., Liang, J., Insinga, A., Eriksen, D., Bjørk, R., … Bahl, C. (2021). Novel design of a high efficiency multi-bed active magnetic regenerator heat pump. *International Journal of Refrigeration*, *132*, 243-254.

Gauß, R., Homm, G., & Gutfleisch, O. (2017). The resource basis of magnetic refrigeration. *Journal of Industrial Ecology*, *21*, 1291-1300.

Greco, A., Aprea, C., Maiorino, A., & Masselli, C. (2019). A review of the state of the art of solid-state caloric cooling processes at room-temperature before 2019. *International Journal of Refrigeration*, *106*, 66-88.

Inmetro. (2011, January). *Portaria n.º 007 - requisitos de avaliação da conformidade para condicionadores de ar.* (Tech. Rep.). INMETRO.

Inmetro. (2012, November). *Portaria n.º 643 - requisitos de avaliação da conformidade para condicionadores de ar.* (Tech. Rep.). INMETRO.

Inmetro. (2013, August). *Portaria n.º 410 - requisitos de avaliação da conformidade para condicionadores de ar.* (Tech. Rep.). INMETRO.

ISO-5151. (2017). *Non-ducted air conditioners and heat pumps - testing and rating for performance* (Tech. Rep.). ISO.

Kamran, M. S., Ahmad, H. O., & Wang, H. S. (2020). Review on the developments of active magnetic regenerator refrigerators – evaluated by performance. *Renewable and Sustainable Energy Reviews*, *133*, 110247.

Kitanovski, A., Tusek, J., Tomc, U., Plaznik, U., Ozbolt, M., & Poredos, A. (2015). *Magnetocaloric energy conversion, from theory to applications*. Springer.

Lozano, J., Peixer, G., Lorenzoni, A., Hoffmann, G., Silva, M., Dutra, S., … Barbosa Jr., J. (2021). *Unidade magnetocalórica.* (Brazilian Patent No. BR 10 2021 023316. Instituto Nacional de Propriedade Industrial.)

Masche, M., Liang, J., Engelbrecht, K., & Bahl, C. (2022). Performance assessment of a rotary active magnetic regenerator prototype using gadolinium. *Applied Thermal Engineering*, *204*, 117947.

Nakashima, A. T., Fortkamp, F. P., de Sá, N. M., dos Santos, V. M., Hoffmann, G., Peixer, G. F., … Barbosa Jr., J. R. (2021). A magnetic wine cooler prototype. *International Journal of Refrigeration*, *122*, 110-121.

Peixer, G. F. (2020). *Thermodynamic design of a magnetic cooling system for air-conditioning applications.* (Master's thesis, Universidade Federal de Santa Catarina, Florianópolis, Brazil.)

Peixer, G. F., Dutra, S. L., Calomeno, R. S., de Sá, N. M., Lang, G. B., Lozano, J. A., & Barbosa Jr., J. R. (2022). Influence of heat exchanger design on the thermal performance of a domestic wine cooler driven by a magnetic refrigeration system. *Anais da Academia Brasileira de Ciências [online]*., *94*.

Qian, S., Nasuta, D., Rhoads, A., Wang, Y., Geng, Y., Hwang, Y., … Takeuchi, I. (2016). Not-in-kind cooling technologies: A quantitative comparison of refrigerants and system performance. *International Journal of Refrigeration*, *62*, 177 - 192.

Santos, D., Silva, M., Hoffmann, G., Lorenzoni, A., Peixer, G. F., Lozano, J. A., & Barbosa Jr., J. R. (2021, November). Experimental evaluation of the fluid flow management system of a magnetic air conditioner. In *Proceedings of the 26th abcm international congress of mechanical engineering.* Florianópolis, Brazil.

Silva, M. C. R., Rosário, G. S., Dutra, S. L., Capovilla, M., Lima, R., Lorenzoni, A., … Barbosa Jr., J. R. (2021, November). Development and characterization of a calibrated calorimeter to evaluate air conditioning systems. In *Proceedings of the 26th abcm international congress of mechanical engineering.* Florianópolis, Brazil.

Trevizoli, P. V., Christiaanse, T. V., Govindappa, P., Niknia, I., Teyber, R., Barbosa Jr., J. R., & Rowe, A. (2016). Magnetic heat pumps: An overview of design principles and challenges. *Science and Technology for the Built Environment*, *22*, 507–519.

ACKNOWLEDGMENTS

This work was funded by CODEMGE (Development Company of Minas Gerais), EMBRAPII (Brazilian Company for Research and Industrial Innovation) and the INCT (National Institutes of Science and Technology) Program (CNPq Grant No. 404023/2019-3; FAPESC Grant No. 2019TR0846).